Determining the nonparabolicity factor of the CdO conduction band using indium doping and the Drude theory

2012 J. Phys. D: Appl. Phys. 45 425302

(http://iopscience.iop.org/0022-3727/45/42/425302)

IOP PUBLISHING JOURNAL OF PHYSICS D: APPLIED PHYSICS

J. Phys. D: Appl. Phys. **45** (2012) 425302 (7pp) doi:10.1088/0022-3727/45/42/425302

Determining the nonparabolicity factor of the CdO conduction band using indium doping and the Drude theory

Rueben J Mendelsberg[1,2], **Yuankun Zhu**[1,3] **and André Anders**[1]

[1] Lawrence Berkeley National Laboratory, Plasma Applications Group, Berkeley, CA, USA
[2] Argonne National Laboratory, Materials Science Division, Argonne, IL, USA
[3] Harbin Institute of Technology, Harbin, People's Republic of China

E-mail: aanders@lbl.gov

Received 10 July 2012, in final form 22 August 2012
Published 1 October 2012
Online at stacks.iop.org/JPhysD/45/425302

Abstract

Due to their high intrinsic electron mobility, CdO-based materials are gaining interest as transparent conductive oxides. By creating model dielectric functions based on the Drude theory, accurate fits to the measured transmittance and reflectance of CdO and CdO : In thin films were achieved without using a frequency dependent Drude damping parameter. Difference in the model between undoped and In-doped CdO showed that the Burstein–Moss shift is not the only mechanism which improves the transparency in In-doped samples. Comparing the Drude analysis with Hall measurements revealed a nonlinear relationship between the free-electron effective mass and the carrier concentration, an effect which is caused by the nonparabolicity of the CdO conduction band. Analysis of 50 CdO : In thin films grown by pulsed filtered cathodic arc showed the nonparabolicity factor was $C = (0.5 \pm 0.2)\,\mathrm{eV}^{-1}$ and the band-edge effective mass was $(0.16 \pm 0.05)m_e$. Knowledge of the effective mass allows for optical measurements of carrier mobility, which was less than or equal to the measured Hall mobility in these films due to the large electron mean free path compared with the grain size.

(Some figures may appear in colour only in the online journal)

1. Introduction

Transparent conductive oxides (TCOs) have been studied for decades and are now well ingrained in our daily lives. Nevertheless, many groups around the world continue researching TCOs in order to further increase the materials' performance and expand the possible applications. Furthermore, some basic material properties are unknown or are still debated, such as the exact role of oxygen vacancies in ZnO and In_2O_3 : Sn. Developing a complete understanding of the common TCOs is a key step towards engineering new materials with superior qualities.

One of the first metal oxides to be investigated was the naturally n-type CdO [1, 2]. However, when the market for transparent conductors exploded, CdO and other toxic Cd-containing oxides were all but abandoned in favour of the nontoxic zinc-, indium- and tin-based oxides. Nevertheless, research into Cd-based TCOs has recently picked up, mainly in response to the development of high efficiency thin-film solar cells which already contain a significant amount of Cd [3]. Much progress has already been made and doped CdO thin films with resistivities below $10^{-4}\,\Omega\,\mathrm{cm}$ and visible transparency above 80% can be readily deposited by several techniques [4–9].

Practical applications aside, CdO is an excellent material in which to study fundamental physics of degenerate semiconductors. Even high purity CdO is typically degenerate (Fermi level within the conduction band) since oxygen vacancies are shallow double donors with a low formation energy under both Cd- and O-rich growth conditions [10]. Carrier concentration (n) for undoped CdO is usually in the 10^{19}–$10^{20}\,\mathrm{cm}^{-3}$ range, but it can be pushed above $10^{21}\,\mathrm{cm}^{-3}$ by doping with various elements [8, 9, 11]. Aside from the Burstein–Moss [12] shift and band-gap renormalization [13],

increasing n in CdO also alters the effective electron mass since the conduction band of CdO is nonparabolic [14]. Several groups have already studied the nonparabolicity of the CdO conduction band [4, 6, 15], but developing a more complete picture is important for most applications of CdO since nonparabolicity affects both the electronic transport and optical properties [16].

In this work, we develop a simple model for the dielectric function of nominally undoped and In-doped CdO (ICO) which is based on the Drude theory. The model was used to fit the optical transmittance and reflectance of 50 high quality ICO thin films with carrier concentrations ranging from 6×10^{19} to $1.5 \times 10^{21}\,\mathrm{cm}^{-3}$. By comparing the extracted Drude parameters with Hall effect measurements, the nonparabolicity factor of the ICO conduction band was inferred using readily available optical and electrical measurements.

2. Film growth and characterization

Pulsed filtered cathodic arc (PFCA) [8, 17] was used to deposit all the CdO samples investigated in this study. Separate Cd and In cathodes were alternately pulsed in order to control the doping level, as described in earlier work [8]. Energy dispersive x-ray spectroscopy (EDX) showed that the In content was between 0 and 9 at%. Most of the films were about 240 nm thick and several thicker samples (≈600 nm) were also produced but had very similar electrical properties. Details of the structural, electrical and optical properties of many such PFCA-deposited CdO : In (ICO) thin films, as well as more information about the equipment which was used can be found in [8].

The samples analysed in this study were deposited on borosilicate glass microscope slides, with a few samples deposited onto c-axis sapphire. Similar quality films were obtained on both substrates, in stark contrast to what has been observed for ICO grown by pulsed laser deposition [18]. Before deposition, the substrate temperature was typically about 230 °C, although some substrates were kept at room temperature or heated to as high as 400 °C. Optimized oxygen partial pressure in our deposition system was typically 1 Pa but a few samples were deposited at pressures as low as 0.4 Pa.

Electrical properties of the samples were subsequently measured with an Ecopia HMS-3000 Hall Measurement System with a 0.6 T magnetic field. Carrier concentration was in the $n_\mathrm{H} = 10^{19}\,\mathrm{cm}^{-3}$ range in the undoped CdO and $n_\mathrm{H} = 10^{20}$–$10^{21}\,\mathrm{cm}^{-3}$ in the doped samples. Optical transmitance (T) and reflectance (R) were recorded from 250 to 2500 nm using a Perkin-Ellmer Lambda 950 dual-beam spectrophotometer equipped with a universal reflectance accessory. No blank substrate was used in the reference path so the collected transmittance is the *absolute* transmittance of the ICO/glass stacks. Reflectance was taken using unpolarized light at 8° incidence in the absolute reflectance mode. The T and R data of each of the 50 samples were then fit with the SCOUT modelling software (www.wtheiss.com) in a very similar fashion as in [19] using a two layer model (film on substrate). Film thickness was determined from step profilometry and confirmed by the T and R fits.

3. Optical model

Excellent fits to the measured T and R data were obtained for all 50 samples using a relatively simple model for the complex dielectric function. Figure 1 shows examples for a nominally undoped CdO film and several In-doped samples. For the undoped CdO, the model used for the complex dielectric function was

$$\epsilon(\omega) = \epsilon_\mathrm{B} + \epsilon_\mathrm{BG}(\omega) + \epsilon_\mathrm{UV}(\omega) + \epsilon_\mathrm{VIS}(\omega) + \epsilon_\mathrm{D}(\omega), \qquad (1)$$

where ω is the frequency and ϵ_B is the dielectric background constant. ϵ_B is similar in value to the high-frequency dielectric background constant (ϵ_∞) but not exactly equal since the other terms in equation (1) can also contribute to the high-frequency optical response. Here, 'high frequency' refers to frequencies much higher than the phonon modes and thus includes the visible and NIR portions of the spectrum.

In this work, the main focus of the dielectric model (equation (1)) is the contribution of the free carriers. In transparent conductors, the Drude theory is a simple yet accurate framework which describes the free-electron photon interaction via

$$\epsilon_\mathrm{D}(\omega) = -\frac{\omega_\mathrm{P}^2}{\omega^2 + \mathrm{i}\omega\Gamma}, \qquad (2)$$

where ω_P is typically called the plasma frequency and Γ is the damping constant (relaxation frequency). However, when written as equation (2), ω_P should be called the Drude frequency and it is related to the longitudinal plasma frequency by the approximation [19] $\omega_\mathrm{Plasma}^2 = \omega_\mathrm{P}^2/\epsilon_\infty - \Gamma^2$. In fact, ω_P and Γ are *angular* frequencies and so the units of ω_P and Γ are $\mathrm{rad\,cm}^{-1}$ when using wavenumbers (cm^{-1}) for the frequency variable. As such, when using equation (2), the free carrier concentration (in cm^{-3}) is calculated using $n = 4\pi^2 c^2 \epsilon_0 m^* \omega_\mathrm{P}^2/100e^2$ where c is the speed of light, ϵ_0 is the permittivity of free space, m^* is the effective carrier mass and e is the elementary charge. Similarly, carrier mobility (μ) is found from $\mu = 100e/2\pi c m^* \Gamma$. This Drude-style model of free carrier interaction is significantly simpler than the rigorous approach used by Hamberg and Granqvist [19], but it has proven to be effective for a wide range of metals and semiconductors.

Equation (2) works well for doped ZnO and In_2O_3 : Sn provided that a frequency-dependent Γ is used [20–22]. It is well accepted that ionized impurity scattering causes such a $\Gamma(\omega)$, giving rise to a frequency dependence which approximates a power law in the visible and NIR range [19, 23]. However, in both CdO and ICO, it is not necessary to use a frequency-dependent Γ in ϵ_D to get good fits to the T and R data from 250 to 2500 nm. This could be due to the relatively high value of ϵ_∞ in CdO, which can screen the carriers from the charged defects. Such a screening effect is clearly visible for the chalcogenides [24], nanocrystals of which show very symmetric localized surface plasmon resonances [25, 26], in stark contrast to those observed in In_2O_3 : Sn nanocrystals [27]. In any case, a more detailed experimental and theoretical study into the carrier scattering mechanisms in doped and undoped CdO would be very beneficial.

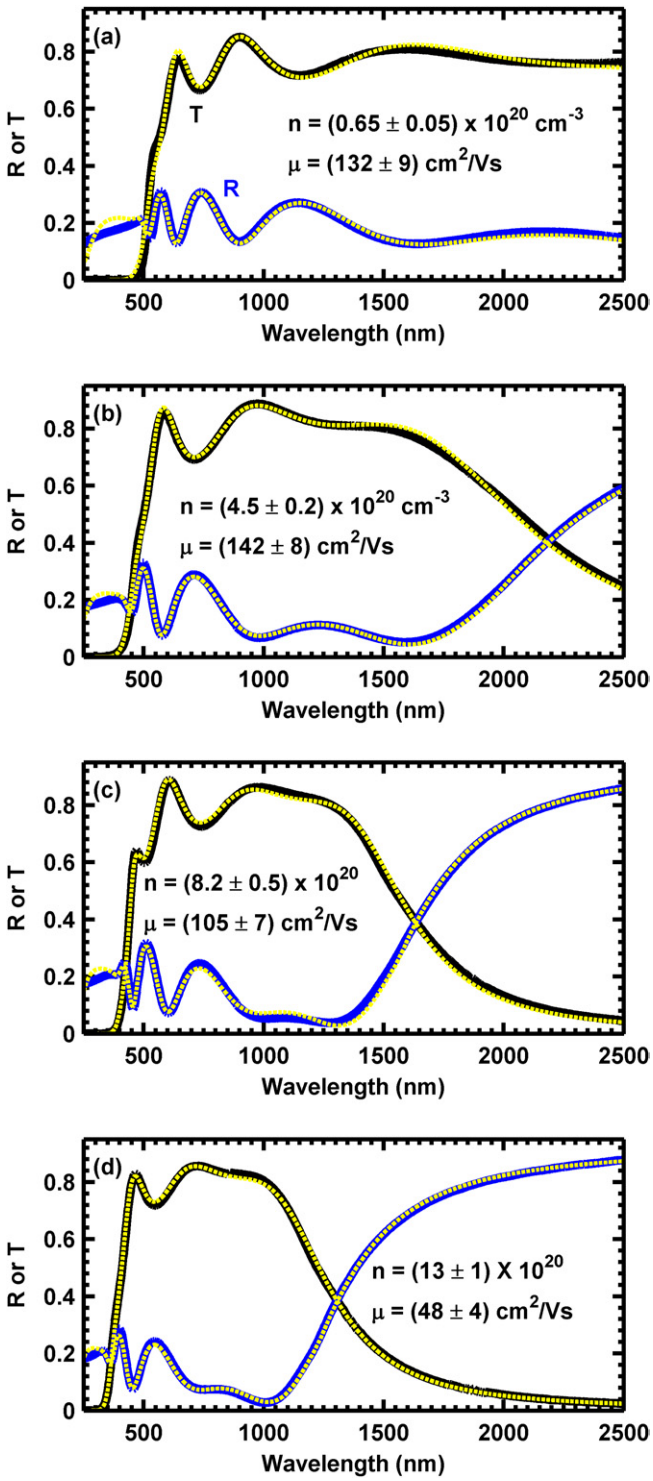

Figure 1. Transmittance (black) and reflectance (blue) of CdO with a wide range of In contents: (*a*) 400 nm of nominally undoped CdO, (*b*) 230 nm of ICO with (1.4 ± 0.4) at% In (*c*) 240 nm with (2.2 ± 0.7) at% In, and (*d*) 200 nm with (9 ± 1) at % In. The dashed yellow lines show the best fits.

Even though we are focused on the Drude term, the other contributions to ϵ in equation (1) need to be accounted for appropriately to get an accurate estimation of ω_P, Γ and film thickness. This is because the observed (screened) plasma absorption feature also depends on the high-frequency dielectric background constant [19] (ϵ_∞). More specifically, the extracted ω_P depends on the dielectric background in the visible–NIR region which is caused by the tail end of the bandgap and any other absorption features.

Fortunately, for thin films the interference fringes provide valuable information needed to accurately determine the dielectric background in the region of ω_P. The positions of the interference minima and maxima and the intensity of the modulation are two important pieces of information, as can be explored when determining film thickness using the well-established envelope method [28]. Modelling the bandgap contribution, ϵ_{BG}, using the O'Leary–Johnson–Lim (OJL) model [29] allows for good fits to the UV absorption as well as for the interference fringes in the visible spectrum. The OJL model was developed for amorphous semiconductors with parabolic bands and exponential tail states. It is only used here to approximate the magnitude and shape of the electronic susceptibility due to the bandgap transition. In other words, using the OJL model for ϵ_{BG} is effective but the extracted parameter values have little or no physical meaning.

Two broad absorption features were also needed alongside ϵ_{BG} to accurately model the undoped CdO data; one in the UV range (ϵ_{UV}) and one in the visible (ϵ_{VIS}). Both were modelled using Kim oscillators as described in previous work [20]. The UV absorption is likely necessary due to the limitations of the OJL model or, alternatively, the presence of absorption into a second conduction band. This term has previously been included when modelling $In_2O_3:Sn$ and $ZnO:Al$ thin films [20, 21, 30]. Intraband or defect related absorption could be responsible for ϵ_{VIS}, but the presence of the weak indirect CdO bandgap [10, 31] near 1 eV could also be contributing. Without ϵ_{UV} and ϵ_{VIS}, poor fits to the undoped CdO spectra were obtained.

In an important contrast, neither ϵ_{UV} nor ϵ_{VIS} were needed to successfully model the data from any of the doped samples. Despite adding six additional free parameters, keeping ϵ_{UV} and ϵ_{VIS} in the model did not significantly reduce the mean square error of the fit for the doped samples. For degenerate carrier concentrations, doping distorts the band structure [32], which may coincidentally hide the absorption responsible for ϵ_{UV}. Doping could also be passivating an optically active native defect responsible for ϵ_{VIS}. Moreover, first-principles calculations suggest that mixing of the In and Cd 5s orbitals creates a hybridization gap within the conduction band, reducing intraband absorptions in the visible spectrum [33]. At this stage, it is unclear why In-doping negates the need for ϵ_{UV} and ϵ_{VIS}, but it seems to make ICO a nearly ideal TCO from both a theoretical and practical perspective.

4. Discussion

The effectiveness of the optical models we chose for CdO and ICO can be seen by the approximately linear plot of n_H versus ω_P^2 shown in figure 2. Perfectly linear behavior would, in fact, indicate a parabolic conduction band and good linearity is indeed observed in our data. The slope of the best fit line which accounts for the measurement uncertainties gives $m^* = (0.42 \pm 0.01)m_e$.

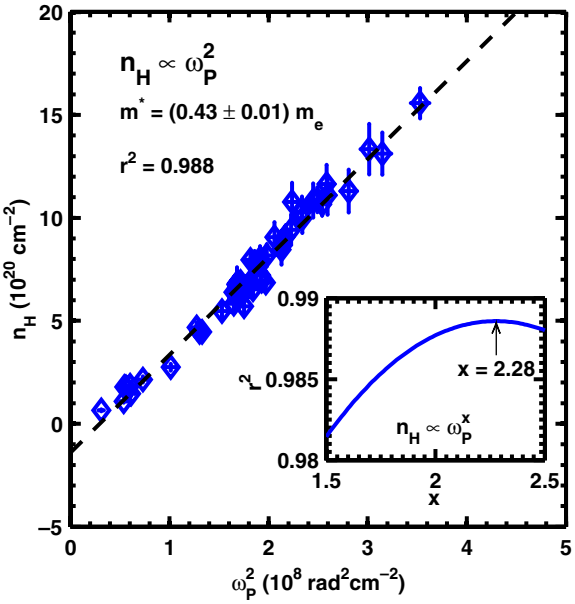

Figure 2. Comparison of the Drude frequency (ω_P) extracted from full modelling of the T and R spectrum to the carrier concentration determined from Hall measurements for all 50 ICO samples. The inset shows the goodness of fit parameter (r^2) for various x values when fitting a straight line to n_H versus ω_P^x.

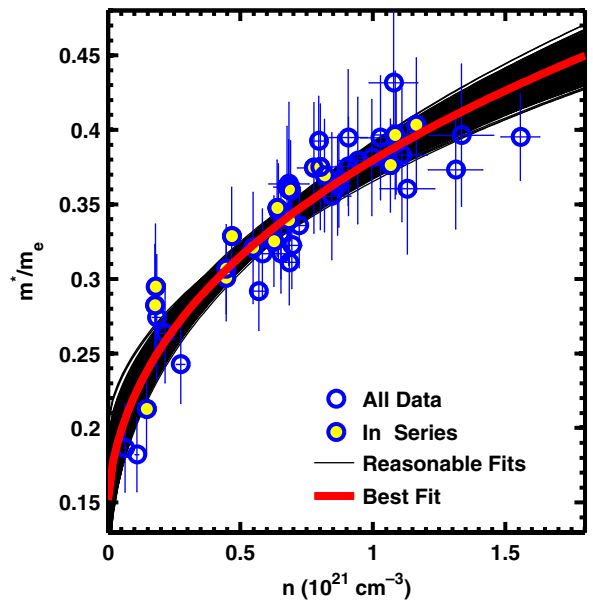

Figure 3. Effective mass (m^*) of 50 CdO samples with In content ranging from 0 to 9 at% The solid red line is the best fit of equation (4) which yields $m_0^* = (0.16 \pm 0.05)m_e$ and $C = (0.5 \pm 0.2)$.

This value is substantially higher than the 0.2 to $0.3m_e$ expected for single crystal CdO epilayers, [15] polycrystalline bulk, [6], and chemical vapor deposited thin films [4] with similar n. However, fitting straight lines to n_H versus ω_P^x for a surprisingly large range of x gives excellent linearity, as shown in the inset of figure 2. As such, care should be taken when using n_H versus ω_P^2 plots for new materials, or when assuming exponents in any relation in general.

Thus, instead of using the slope from figure 3, m^* was calculated for each sample from ω_P determined from the optical model and n measured by the Hall technique. Figure 3 shows the results and a seemingly nonlinear variation of m^* with increasing n is observed for these arc-deposited thin-films. Past $m^*(n)$ measurements [4, 6] on doped and undoped CdO show a linear dependence of m^* on n. However, the previous reports may not have explored high enough n to observe the nonlinearity (as in [6, 34]) or possibly did not have quite enough data points or errorbars (in the case of [4]).

To further explore potential nonlinearity in $m^*(n)$, we followed the lines of Pisarkiewicz and Kolodziej [16], which was later utilized by Ruske *et al* [34]. A quadratic term is added to the dispersion relation of the conduction band such as

$$\frac{\hbar^2 k^2}{2m_0^*} = E + CE^2, \tag{3}$$

where E is the electron energy for wavevector k, m_0^* is the electron effective mass at the conduction band minimum and C is the nonparabolicity factor. Using this conduction band model, the dependence of m^* on n is given by [16]

$$m^* = m_0^* \sqrt{1 + 2C\frac{\hbar^2}{m_0^*}\left(3\pi^2 n\right)^{2/3}}, \tag{4}$$

which was used to find the best fit through all the data as shown by the solid red line in figure 3.

Now, one can argue that the data shown in figure 3 are essentially linear ($r^2 = 0.87$) using the reverse of the argument presented in figure 2. Thus, it is important that upper and lower bounds to both m_0^* and C are obtained in order to establish the validity of equation (4). However, many algorithms used for nonlinear fitting give upper and lower bounds on the fitting parameters which are solely based on the statistical spread of the data from the best fit line. In this work, an iterative Monte Carlo style method [35] was used which accounts for the measurement uncertainties and works well for linear least-squares fitting (see appendix A in [36]). The main assumptions are (1) systematic errors are negligible and (2) the true value of each data point is anywhere within the upper and lower errorbar with equal probability. Instead of using the measured values (the markers in the figure), the value of each data point passed into the nonlinear fitting algorithm was randomly selected from the box defined by the measured value and the m^* and n errorbars. Then, the best fit was found and the process was repeated 1000 times for the data shown in figure 3, taking a total of about 300 s on a dual core 2.5 GHz laptop. The best fit parameters were the averages from all the iterations and we used the minimum and maximum values to indicate the upper and lower bounds.

Using all the data points, a physically reasonable value of $m_0^* = (0.16 \pm 0.05)m_e$ was obtained from the algorithm, which agrees well with values suggested in previous work [4, 6, 36]. No other analysis using equation (4) has been carried out on CdO thus far, but the best fit value for the nonparabolicity factor, $C = (0.5 \pm 0.2)\,\mathrm{eV}^{-1}$, is in between $C = 0.3\,\mathrm{eV}^{-1}$ found [34] for ZnO : Al and the $C = 1\,\mathrm{eV}^{-1}$ found [16] for SnO_2. Very reasonable uncertainty bounds were obtained for both m_0^* and C indicating that equation (4) gives a good

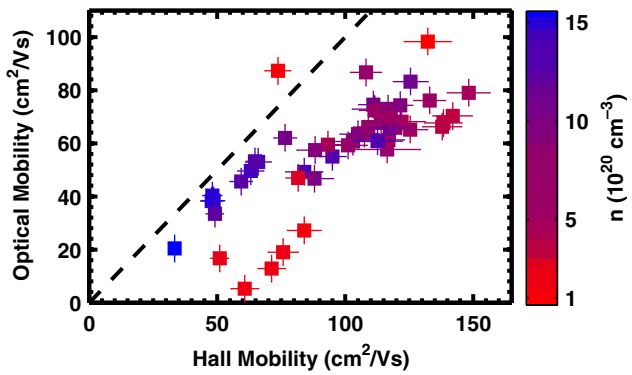

Figure 4. Comparison of the carrier mobility measured by Hall and that extracted from the optical data. The colour of the marker goes from blue for high n to red for low n. The dotted line is $y = x$.

approximation of $m^*(n)$ in CdO and equation (3) is a good way to account for the nonparabolicity in the CdO conduction band.

Using the same methodology on a large number of ZnO : Al thin films, Ruske *et al* [34] showed that variations in key growth conditions lead to significant smearing of the $m^*(n)$ relationship. Samples about 230 nm thick with varying In content, but grown on glass under the same optimized oxygen partial pressure (1 Pa) and relatively low substrate temperature (230 °C) are shown as the solid markers in figure 3 (In-series). This series of samples lies neatly along the best fit line through all the data. Using just the In-series, the best fit parameters are $m_0^* = (0.17 \pm 0.5)m_e$ and $C = (0.5 \pm 0.2)\,\mathrm{eV}^{-1}$, which gives essentially the same parameter values and uncertainty bounds. Thus, the accuracy of the fit to our data is limited mainly by the uncertainty in the measurements and is less influenced by the spread caused by variations of the growth conditions.

Now that we have a good idea about the variation of m^* with n, the Γ values extracted from the Drude modelling can be used to calculate μ. A comparison of μ measured by Hall to those calculated from Γ is shown in figure 4. The optical mobility is notably lower than the Hall mobility, in contrast to the results of a recent mid-IR reflectance study on undoped CdO [37]. Usually, optical mobility is larger than Hall mobility for polycrystalline thin films [37–39] since the electrons do not typically cross grain boundaries during their plasmonic oscillations. However, XRD measurements indicate [8] the average grain size in these arc-grown films is no larger than 40 nm. From the Hall measurements, the electron mean free path can be estimated [40] and was in the range 10–30 nm for the arc-grown ICO. Thus, its likely that many electrons are crossing the grain boundaries during optical excitation, which will bring the optical mobility closer to the Hall mobility.

From figure 4 it can be seen that the agreement between the optical and Hall mobility seems to improve with increasing n. This is most likely due to the fact that for higher n more of the plasmon absorption feature is observable in the 250–2500 nm spectral range, leading to more accurate estimates of the plasmon damping and hence carrier mobility. Thus, the y-error bars shown in figure 4 are likely underestimated for the films with relatively low n. Going to longer wavelengths would allow more solid conclusions about carrier mobility to be made. Another possible avenue for improvement is to explore the more rigorous theories dealing with carrier scattering [19, 22] and how they apply to CdO-based TCOs.

5. Conclusion

The Drude theory is an excellent foundation to build up an understanding of the optical and electrical properties of doped and undoped CdO thin films. Surprisingly, there was no need to account for ionized impurity scattering to accurately fit the T and R data, which is in contrast to In_2O_3 : Sn and doped ZnO and is possibly due to the high dielectric background for CdO. Furthermore, two absorption features which were necessary to model the undoped-CdO data were not needed for the In-doped samples. Thus, the improvement in the optical transparency in CdO due to In doping is not solely due to the bandgap widening from the Burstein–Moss shift.

By combining the Drude analysis with Hall measurements, the effective electron mass was determined as a function of carrier concentration. Nonlinear behavior was observed for $m^*(n)$ which was fit well using the theory of Pisarkiewicz and Kolodziej. Best fit parameters were $m_0^* = (0.17 \pm 0.5)m_e$ for the conduction band-edge effective mass and the nonparabolicity factor was $C = (0.5 \pm 0.2)\,\mathrm{eV}^{-1}$. The Monte Carlo style variation of nonlinear least-squares fitting used in this work showed that the measurement uncertainties in m^* and n were the main contribution to the uncertainties in m_0^* and C as opposed to uncertainty due to the statistical spread of the data or fluctuations under the growth conditions. Improving these measurement uncertainties would likely require modelling a larger spectral region of the T and R data or integrating more electrical measurements into the analysis.

Once m^* was determined, the optical carrier mobility calculated from the Drude relaxation frequency was compared with the Hall mobility. Surprisingly, the optical mobility was significantly lower than Hall measurements for most samples. However, comparable optical and Hall mobilities can be expected when the electron mean free path is large and the grain size is small, as is the case for the arc-deposited CdO used in this work. Nevertheless, the measurements did not likely go far enough into the IR to make sound conclusions about the carrier mobility in many of the samples, particularly at low carrier concentration when less of the plasmonic optical absorption feature is observed. Understanding and improving the carrier mobility in doped CdO are very important for its electronic applications and requires properly accounting for the nonparabolicity of the conduction band.

Acknowledgments

The authors would like to thank K M Yu, D J Milliron, J Zhu and J Han. Research was supported by the LDRD Program of Lawrence Berkeley National Laboratory, by the Assistant Secretary for Energy Efficiency and Renewable Energy, Office of Building Technologies under US Department of Energy Contract No DE-AC02-05CH11231. Additional support was provided by the National Natural Science Foundation of China (Grant Nos 51072039 and 50972031), and the PhD

Programs Foundation of the Ministry of Education of China (20112302110036).

References

[1] Bidwell C C 1914 Thermal electromotive forces in oxides *Phys. Rev.* **3** 204–16

[2] Holland L and Siddall G 1953 The properties of some reactively sputtered metal oxide films *Vacuum* **3** 375

[3] Garland J W, Biegala T, Carmody M, Gilmore C and Sivananthan S 2011 Next-generation multijunction solar cells: the promise of II–VI materials *J. Appl. Phys.* **109** 102423

[4] Coutts T J, Young D L, Li X, Mulligan W P and Wu X 2000 Search for improved transparent conducting oxides: a fundamental investigation of CdO, Cd_2SnO_4, and Zn_2SnO_4 *J. Vac. Sci. Technol.* A **18** 2646–60

[5] Dakhel A A 2008 Influence of hydrogenation on the electrical and optical properties of CdO : Tl thin films *Thin Solid Films* **517** 886–90

[6] Dou Y, Egdell R G, Walker T, Law D S L and Beamson G 1998 N-type doping in CdO ceramics: a study by EELS and photoemission spectroscopy *Surf. Sci.* **398** 241–58

[7] Jin S *et al* 2008 Tuning the properties of transparent oxide conductors. Dopant ion size and electronic structure effects on CdO-based transparent conducting oxides. Ga- and In-doped CdO thin films grown by MOCVD *Chem. Mater.* **20** 220–30

[8] Zhu Y-K, Mendelsberg R J and Anders A 2012 Indium doped cadmium oxide thin films prepared by pulsed filtered cathodic arc deposition for multi-junction solar cell applications *Appl. Surf. Sci.* (in review)

[9] Maity R and Chattopadhyay K K 2006 Synthesis and characterization of aluminum-doped CdO thin films by sol–gel process *Sol. Energy Mater. Sol. Cells* **90** 597–606

[10] Burbano M, Scanlon D O and Watson G W 2011 Sources of conductivity and doping limits in CdO from hybrid density functional theory *J. Am. Chem. Soc.* **133** 15065–72

[11] Gupta R K, Ghosh K, Patel R and Kahol P K 2009 Highly conducting and transparent Ti-doped CdO films by pulsed laser deposition *Appl. Surf. Sci.* **255** 6252–55

[12] Burstein E 1954 Anomalous optical absorption limit in InSb *Phys. Rev.* **93** 632–33

[13] Jain S C and Roulston D J 1991 A simple expression for band gap narrowing in heavily doped Si, Ge, GaAs and Ge_xSi_{1-x} strained layers *Solid State Elec.* **34** 453–65

[14] Koffyberg F P 1969 Carrier concentration in oxygen deficient CdO single crystals *Phys. Lett.* A **30** 37–8

[15] Jefferson P H, Hatfield S A, Veal T D, King P D C, McConville C F, Zúñiga Pérez J and Muñoz Sanjosé V 2008 Bandgap and effective mass of epitaxial cadmium oxide *Appl. Phys. Lett.* **92** 022101

[16] Pisarkiewicz T and Kolodziej A 1990 Nonparabolicity of the conduction band structure in degenerate tin dioxide *Phys. Status Solidi* B **158** K5–K8

[17] Anders A, Lim S H N, Yu K M, Andersson J, Rosén J, McFarland M and Brown J 2010 High quality ZnO:Al transparent conducting oxide films synthesized by pulsed filtered cathodic arc deposition *Thin Solid Films* **518** 3313–19

[18] Yan M, Lane M, Kannewurf C R and Chang R P H 2001 Highly conductive epitaxial CdO thin films prepared by pulsed laser deposition. *Appl. Phys. Lett.* **78** 2342–44

[19] Hamberg I and Granqvist C G 1986 Evaporated Sn-doped In_2O_3 films—basic optical-properties and applications to energy-efficient windows *J. Appl. Phys.* **60** R123–59

[20] Mendelsberg R J, Garcia G and Milliron D J 2012 Extracting reliable electronic properties from transmission spectra of metal oxide thin films and nanocrystal films by careful application of the Drude theory *J. Appl. Phys.* **111** 063515

[21] Mergel D and Qiao Z 2002 Dielectric modelling of optical spectra of thin In_2O_3 : Sn films *J. Phys. D: Appl. Phys.* **35** 794–801

[22] Pflug A, Sittinger V, Ruske F, Szyszka B and Dittmar G 2004 Optical characterization of aluminum-doped zinc oxide films by advanced dispersion theories *Thin Solid Films* **455–456** 201–6

[23] Gerlach E 1986 Carrier scattering and transport in semiconductors treated by the energy-loss method *J. Phys. C: Solid State Phys.* **19** 4585–603

[24] Maslowska A 1987 The Burstein absorption-edge structure in lead chalcogenides *Phys. Status Solidi* B **139** 161–71

[25] Dorfs D, Härtling T, Miszta K, Bigall N C, Kim M R, Genovese A, Falqui A, Povia M and Manna L 2011 Reversible tunability of the near-infrared valence band plasmon resonance in $Cu_{2-x}Se$ nanocrystals *J. Am. Chem. Soc.* **133** 11175–80

[26] Luther J M, Jain P K, Ewers T and Alivisatos P A 2011 Localized surface plasmon resonances arising from free carriers in doped quantum dots *Nature Mater.* **10** 361–66

[27] Mendelsberg R J, Garcia G, Li H, Manna L and Milliron D J 2012 Understanding the plasmon resonance in ensembles of degenerately doped semiconductor nanocrystals *J. Phys. Chem.* C **116** 12226

[28] Swanepoel R 1983 Determination of the thickness and optical constants of amorphous silicon *J. Phys. E: Sci. Instrum.* **16** 1214

[29] O'Leary S K, Johnson S R and Lim P K 1997 The relationship between the distribution of electronic states and the optical absorption spectrum of an amorphous semiconductor: an empirical analysis *J. Appl. Phys.* **82** 3334–40

[30] Qiao Z, Agashe C and Mergel D 2006 Dielectric modeling of transmittance spectra of thin ZnO : Al films *Thin Solid Films* **496** 520–25

[31] Koffyberg F P 1976 Thermoreflectance spectra of CdO: band gaps and band-population effects *Phys. Rev.* B **13** 4470–76

[32] Sernelius B E, Berggren K-F, Jin Z-C, Hamberg I and Granqvist C G 1988 Band-gap tailoring of ZnO by means of heavy Al doping *Phys. Rev.* B **37** 10244

[33] Wang A, Babcock J R, Edleman N L, Metz A W, Lane M A, Asahi R, Dravid V P, Kannewurf C R, Freeman A J and Marks T J 2001 Indium–Cadmium–Oxide films having exceptional electrical conductivity and optical transparency: Clues for optimizing transparent conductors *Proc. Natl. Acad. Sci. USA* **98** 7113–16

[34] Ruske F, Pflug A, Sittinger V, Szyszka B, Greiner D and Rech B 2009 Optical modeling of free electron behavior in highly doped ZnO films *Thin Solid Films* **518** 1289–93

[35] Mendelsberg R J 2009 Photoluminescence of ZnO grown by eclipse pulsed laser deposition *PhD Thesis* University of Canterbury, Christchurch, New Zealand

[36] Finkenrath H, Köhler H and Lochmann M 1966 Optische Eigenabsorption und Dielektrizitatskonstante von Kadmiumoxyd bei hoher Elektronenentartung *Z. Angew. Phys.* **21** 512

[37] Vasheghani Farahani S K, Veal T D, King P D C, Zúñiga Pérez J, Muñoz Sanjosé V and McConville C F 2011 Electron mobility in CdO films *J. Appl. Phys.* **109** 073712

[38] Steinhauser J, Fay S, Oliveira N, Vallat-Sauvain E and Ballif C 2007 Transition between grain boundary and intragrain scattering transport mechanisms in boron-doped zinc oxide thin films *Appl. Phys. Lett.* **90** 142107

[39] Yamada T, Makino H, Yamamoto N and Yamamoto T 2010 Ingrain and grain boundary scattering effects on electron mobility of transparent conducting polycrystalline Ga-doped ZnO films *J. Appl. Phys.* **107** 123534

[40] Yamamoto T, Sakemi T, Awai K and Shirakata S 2004 Dependence of carrier concentrations on oxygen pressure for Ga-doped ZnO prepared by ion plating method *Thin Solid Films* **451** 439–42